# THE RFI SUPPRESSION METHOD BASED ON STFT APPLIED TO SAR

## Tengfei Zhao*, Yongsheng Zhang, Lin Yang, Zhen Dong, and Diannong Liang

School of Electronic Science and Engineering, National University of Defense Technology, Changsha, Hunan 410073, China

**Abstract**—Improved radio frequency interference suppression method based on short time Fourier transform applied to synthetic aperture radar is proposed in this paper. The radio frequency interference, including narrow-band interference and wide-band interference, are analyzed in time frequency domain. The interference is identified at instantaneous frequency spectrum by a novel threshold criterion in time frequency domain, and then an adaptive gain coefficient is determined for instantaneous frequency spectrum at every certain time. The gain coefficient can keep the useful signal correctly during interference suppression. In the end, the performance of the proposed method is demonstrated by the experiment based on the real synthetic aperture radar data adding the interference.

## 1. INTRODUCTION

Synthetic aperture radar (SAR) [1], with the ability of day and night, all weather and climate observation, has bright foreground in both military surveillance and civilian exploration [2–5]. In order to obtain high resolution in range direction, SAR system transmits wide band signal [6]. However, the frequency bands are not reserved exclusively for radar application, and they are also used by other applications, such as frequency modulation broadcast, television and communication. These signals incepted by the SAR receiver will decrease the quality of SAR image seriously. We call these signals radio frequency interference (RFI). The low frequency band SAR, especially the VHF/UHF band SAR, is very sensitive to the RFI influence. Although the SAR uses 2-dimensional matching filtering, which has inherent ability in

interference suppression, the RFI with strong power will still bury useful signal and take on bright stripes along the range direction in SAR images. According to the ratio of interference band to useful signal band, the RFI can be classified into narrow-band interference (NBI) if the ratio is less than 1% and wide-band interference (WBI) if the ratio is greater than 1% [7, 8].

Some methods are proposed for RFI suppression. Based on the notch concept, there are frequency notch filtering [9] and channel equalization [10]. Frequency notch filtering is to detect the contaminated spot in range frequency domain and to process with a notch filter, whereas the frequency notch filtering will lead to the gap of signal spectrum. To design an adaptive gain coefficient for the signal frequency spectrum, channel equalization can keep the useful signal while RFI is suppressed. However, channel equalization performs well in the stationary interference suppression but poorly in non-stationary interference suppression. The adaptive least mean square (LMS) filtering [11] is to estimate the interference, and then subtract from the echo data. However, that will lead to high sidelobe. Making use of the orthogonality of the useful signal subspace and interference subspace, interference can be obtained by projecting the echo signal to interference subspace, and then subtracting the interference from echo data [7, 12]. However, the precision of interference subspace construction will influence the interference suppression effect. Based on the empirical mode decomposition (EMD) theory [13, 14], the echo signal can be decomposed into a series of intrinsic mode functions (IMFs), and then the IMFs corresponding to the interference are subtracted from the echo signal. However, it is difficult to exactly distinguish the IMFs corresponding to the interference, which will lead to large interference residuals or severe signal distortion. Based on the SAR images, [15] proposes the subband spectral cancellation (SSC): dividing the SAR images into subbands, the RFI can be assumed by subband signal subtracting, approximately. Then remove the RFI in SAR image by subtraction. Interference suppression method for focused SAR images is proposed in [16]. The methods based on SAR images are suitable for specific interference mode. In addition, there are other methods mentioned in [17–19]. However, these methods mostly make use of the narrow band characteristic of interference, and they may not be suitable for the WBI suppression.

Based on most SAR echoes with RFI, the interference takes on spikes in the instantaneous frequency spectrum [7]. For the instantaneous frequency spectrum estimation of stationary and non-stationary signals, short time Fourier transform (STFT) is an effective tool for time frequency analysis. The RFI suppression method

proposed in [8] is the estimation of the instantaneous frequency spectrum by STFT. The strong interference takes on spikes in the instantaneous frequency spectrum, and then the wavelet transform is used to detect the spike and remove it. In spite of the good performance of the method proposed in [8] for NBI and WBI suppression, the twice transforms will lead to a very high computation load. Because the interference mostly takes on spikes in instantaneous frequency spectrum, it can be captured directly without wavelet transform, and this will greatly improve the computation efficiency. An improved method based on STFT is proposed in this paper. In time frequency domain, the wavelet transform is replaced with a novel method named maximum mean ratio (MMR) for RFI detection. An adaptive gain coefficient for instantaneous frequency spectrum is derived at every certain time, and it will keep the useful signal correctly during RFI suppression. The approach proposed in this paper has much lower computation load than the approach proposed in [8], and the performance of the proposed approach is demonstrated by both NBI and WBI suppression.

This paper is arranged as follows. Section 2 gives a brief introduction of model of RFI and STFT. Section 3 introduces the principle of RFI suppression based on STFT. Section 4 gives the experimental results and analysis and is followed by the conclusion.

## 2. MODEL OF RFI AND STFT

### 2.1. Model of RFI

After the orthogonal demodulation and A/D transform, the SAR echo [7] can be expressed as

$$x(n) = s(n) + noi(n) + rfi(n), \quad n = 1, \ldots, N \tag{1}$$

where $s$, $noi$ and $rfi$ denote the useful echo signal, thermal noise and interference, respectively; $n$ denotes the time sample; $N$ denotes the number of total time samples.

For the NBI, the model of RFI [20] can be given as

$$rfi(n) = \sum_{p=1}^{P} A_p \exp\left[j(2\pi f_p n + \theta_p)\right] \tag{2}$$

where $A_p$, $f_p$ and $\theta_p$ denote the amplitude, frequency and phase of the complex sinusoid signal, respectively; $P$ denotes the number of the NBI.

With the development of wide-band communication and digital TV, the low-frequency-band SAR, especially the VHF/UHF-band

SAR, is facing with the influence of more and more WBIs, especially the digital video broadcasting-terrestrial (DVB-T). For the WBI, DVB-T interference and linear frequency modulation (LFM) interference are mainly analyzed in this paper. DVB-T [21] system is one of the digital terrestrial television standards which the International Telecommunication Union (ITU) recommends. DVB-T system has higher frequency spectrum utilization by using code orthogonal frequency division multiplexing (COFDM). There are three modulation modes: quadrature phase shift keying (QPSK), 16 quadrature amplitude modulation (16QAM) and 64 quadrature amplitude modulation (64QAM); four guard interval $T_g$ (1/4, 1/8, 1/16, 1/32). There are two subcarrier modes: 2 K and 8 K in the 8 MHz bandwidth. The 2 K mode has 1705 subcarriers, and the 8 K mode has 6817 subcarriers. This paper talks about the 8 K mode. The DVB-T signal consists of frame, and every frame has 68 orthogonal frequency division multiplexing (OFDM) symbols. The duration of every frame is $T_F$, and the duration of OFDM symbol is $T_s$. The $T_s$ consists of data part $T_u$ and guard interval $T_g$. Based on [21], the DVB-T signal can be expressed as

$$S_{RF}(n) = \mathrm{Re}\left\{ \exp(j2\pi f_c n) \sum_{m=0}^{\infty} \sum_{l=0}^{67} \sum_{k_{SC}=0}^{6816} c\psi(n) \right\} \tag{3}$$

$$\psi(n) = \begin{cases} \exp\left(\dfrac{j2\pi k(n-T_g-lT_s-68mT_s)}{T_u}\right), & (l+68m)T_s \leq n \leq (l+68m+1)T_s \\ 0, & \text{else} \end{cases} \tag{4}$$

where $f_c$, $m$, $l$ and $k_{SC}$ denote center frequency, frame number, symbol number and subcarrier number, respectively; $n$ denotes the time sample; $k$ denotes the subcarrier number corresponding to $f_c$; $c$ denotes the information modulated on the subcarriers. The DVB-T signal will be incepted by the SAR receiver working in VHF/UHF band. Because of the wide band, the DVB-T signal will affect the useful SAR echo seriously. For the DVB-T WBI, (1) can be given as

$$x(n) = s(n) + noi(n) + S_{RF}(n), n = 1, \ldots, N \tag{5}$$

where $S_{RF}$ denotes the DVB-T interference. For the LFM WBI, (1) can be given as

$$x(n) = s(n) + noi(n) + \sum_{p=1}^{P} A_p \exp[j(2\pi f_p n + \pi k_r n^2)], n = 1, \ldots, N \tag{6}$$

where $A_p$, $f_p$ and $k_r$ denote the amplitude, carrier frequency and the frequency modulation ratio of LFM interference; $P$ denotes the number of LFM interference.

## 2.2. STFT

Using a sliding data window, the STFT can obtain the time frequency characteristic of discretional spot. The STFT spectrum [22] of signal $x(n)$ can be described as

$$X(m,k) = \sum_{n} h(m-n)x(n)\exp(-j2\pi nk/N) \qquad (7)$$

where $m$, $k$, $n$ and $N$ denote the time sample number, frequency sample number, integer index and number of total frequency samples, respectively; $h$ denotes the data window. The inverse short time Fourier transform (ISTFT) can be expressed as

$$x(n) = \frac{1}{NH(0)} \sum_{m} \sum_{k=0}^{N-1} X(m,k)\exp(j2\pi nk/N) \qquad (8)$$

where $H(0) = \sum_{m} h(m-n)$.

In order to locate the interference spot in time frequency domain, good temporal and spectral resolutions are necessary. Generally, rectangular, Hamming and Hanning windows are used for STFT. However, the Heisenberg's uncertainty principle indicates the contradiction between the temporal and spectral resolutions: The narrow data-window will lead to good temporal resolution but poor spectral resolution. In turn, the wide data-window will lead to fine spectral resolution but poor temporal resolution. Hence, there will be a tradeoff between temporal and spectral resolutions. The length of slide window is a critical point. Two concentration measures were introduced in [22].

$$v_1 = -\frac{1}{2} \sum_{m} \sum_{k} \log\left(|X(m,k)|^3\right) \qquad (9)$$

$$v_2 = \left(\sum_{m} \sum_{k} |X(m,k)|^4\right) \Big/ \left(\sum_{m} \sum_{k} |X(m,k)|^2\right)^2 \qquad (10)$$

Renyi information of the third order and the ratio of 4 norm to 2 norm of the $X(m,k)$ can place much of the signal energy into a small region in the time frequency domain. It is recognized that the high values of $v_1$ and $v_2$ reflect good time and frequency concentration.

The length of LFM signal is set to 2304 samples. The signal noise ratio (SNR) is 10 dB. Figures 1(a)–(c) depict the time frequency spectrum of LFM signal using Hamming window with three window length. Figures 1(d)–(f) show the values of two concentration measures as functions of the window length using Hamming, Hanning and
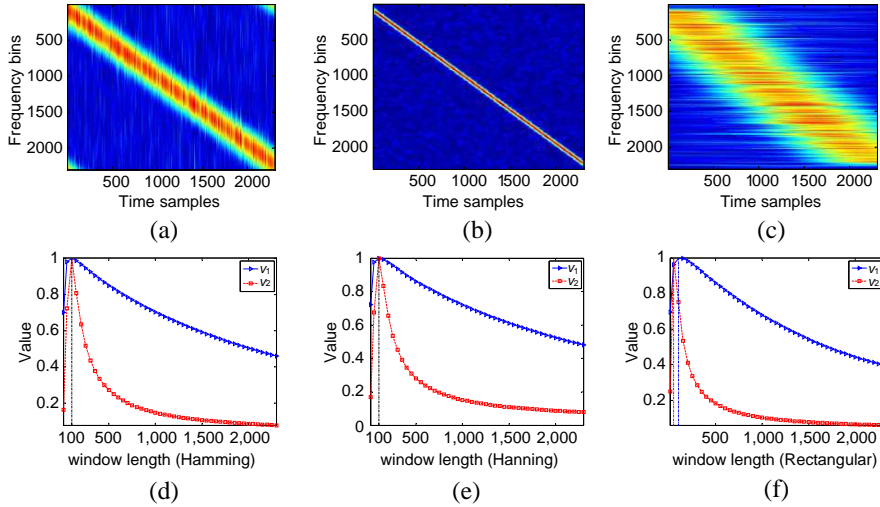
**Figure 1.** Concentration measures for LFM signal. (a) Window length = 10 (Hamming). (b) Window length = 100 (Hamming). (c) Window length=2300 (Hamming). (d) Concentration measures with Hamming window. (e) Concentration measures with Hanning window. (f) Concentration measures with rectangular window.

rectangular windows, respectively. In Figures 1(d) and (e), the maximum values of $v_1$ and $v_2$ can be reached when the window length is 100 samples. However, the maximum values of $v_1$ and $v_2$ cannot be reached at the same window length using rectangular window (Figure 1(f)). It is obvious that the time frequency spectrum using the Hamming window with the length of 100 samples is more concentrated than the Hamming window with the length of 10 and 2300 samples (Figures 1(a)–(c)). In this paper, the Hamming window is adopted. The STFT window length is set to 100 samples for LFM WBI in terms of the signal length (2304 samples). In addition, the tone NBI takes on bright line along the time axis in time frequency spectrum, and DVB-T WBI (the superposition of many complex sinusoid signals) takes on wide bright stripe along the time axis in time frequency spectrum. Hence, the higher spectral resolution comes with the more concentration of the tone NBI and the DVB-T WBI. However, considering the computation efficiency, the STFT window length is set to the quarter of the signal length for tone NBI and DVB-T WBI suppression.

## 3. RFI SUPPRESSION BASED ON STFT

In the time frequency domain, the interference spot can be located correctly. After STFT, the instantaneous frequency spectrum $X(m,:)$ at a certain time $m$-th is obtained. Through the RFI identification and suppression towards all the instantaneous frequency spectrums, the signal RFI suppressed can be obtained by ISTFT.

### 3.1. RFI Identification

Before the RFI suppression, it is important to locate the interference spot. The interference will take on spikes in instantaneous frequency spectrum. Hence, the ratio of maximum amplitude to mean amplitude of instantaneous frequency spectrum can be used to identify the interference. Accordingly, this paper proposes an adaptive threshold criterion called MMR. The MMR is given as

$$R = \max(|X(m,:)|) \bigg/ \frac{1}{N} \sum_{n=1}^{N} |X(m,n)| \tag{11}$$

$$th = \begin{cases} \max(|X(m,:)|), & R < 2 \\ \dfrac{1}{N}\displaystyle\sum_{n=1}^{N}|X(m,n)| + \left\{ \dfrac{1}{N-1}\displaystyle\sum_{n=1}^{N}\left[|X(m,n)| - \dfrac{1}{N}\displaystyle\sum_{n=1}^{N}|X(m,n)|\right]^2 \right\}^{1/2}, & R \geq 2 \end{cases} \tag{12}$$

where $R$ and $th$ denote the MMR and the interference threshold, respectively; $\max(*)$ and $|*|$ denote the maximum value and absolute value, respectively. In order to identify the interference exactly, the MMR needs a reasonable criterion. Furthermore, considering that the interference components that are not correlated with the SAR signal are suppressed by about 30 dB through range compression, and to prevent original signal loss, a 3 dB or more difference is adopted as the criterion between the desired signal and the interference in this case [23]. According to 3 dB, the reasonable criterion is set to 2 for MMR. If $R < 2$, the interference is light, and the maximum amplitude of $X(m,:)$ will be the interference threshold to protect the useful information. If $R \geq 2$, the interference is strong, thus the interference threshold will adopt the sum of mean value and standard deviation. Then the interference spot will be located if the amplitude of instantaneous frequency spectrum is greater than the interference threshold.

### 3.2. RFI Suppression

For the RFI suppression, this paper proposes a method: Construct an adaptive gain coefficient $W = [W(1), W(2), \ldots, W(N)]$ for

instantaneous frequency spectrum at every certain time. $N$ denotes the total number of instantaneous frequency spots at every certain time. The gain coefficient can suppress the interference while protecting the useful information. The construction of gain coefficient will exploit the Gaussian statistic characteristic of the SAR echo [8]. The STFT is a linear operation, thus the Gaussian statistic characteristic is reasonable for the time frequency spectrum. Corresponding to the instantaneous frequency spectrum at the $m$-th time $X(m,:)$, for expression convenience, suppose that the $k$-th instantaneous frequency spot is interference spot (If there are many interference spots in instantaneous frequency spectrum, the components of gain coefficient can be derived one by one in the same way), and then the gain coefficient at the $k$-th instantaneous frequency spot can be obtained as

$$X_k = [|X(m, k-L/2)|, \ldots, |X(m,k)|, \ldots, |X(m, k+L/2-1)|] \quad (13)$$

$$W(k) = mid(X_k)/|X(m,k)| \quad (14)$$

where $L$ and $X_k$ denote the length of data window and amplitude of instantaneous frequency spots around the *k-th* instantaneous frequency spot, respectively; $mid$ denotes the median value (sort the value by ascending, then determine the median value). Because of the Gaussian statistic characteristic of the time frequency spectrum, the median value will be very close to the truth value of the interference spot. The median value will be closer to the truth value of the interference spot with longer data window. For the residual spots of $X(m,:)$ without interference, the gain coefficient at these spots can be set equal to one. Hence, the gain coefficient will only process the interference spots but keep the spots without interference.

$$W(1, \ldots, k-1, k+1, \ldots, N) = \underbrace{[1, 1, \ldots, 1]}_{N-1} \quad (15)$$

where $N$ denotes the length of instantaneous frequency spectrum. Then the instantaneous frequency spectrum at the $m$-th time after RFI suppression can be given as

$$\tilde{X}(m,:) = X(m,:) * W(:) \quad (16)$$

where $\tilde{X}(m,:)$ denotes the instantaneous frequency spectrum at the $m$-th time after RFI suppression. Processing the instantaneous frequency spectrum at every certain time, the SAR echo after RFI suppression will be reconstructed by ISTFT.

## 4. EXPERIMENT AND ANALYSIS

### 4.1. Experiment

The experiment is used to verify the validity of the proposed method. Because of the difficulty in obtaining the real SAR data with RFI, we will use other way to get the experimental SAR data with RFI: Adding the simulated RFI data to the SAR raw data. The real RadarSat-1 data are used to be SAR raw data. In order to testify the validity of the proposed method for both NBI and WBI suppression, the simulated NBI and WBI (LFM interference with 5 MHz bandwidth and DVB-T interference with 8 MHz bandwidth) data are added to the RadarSat-1 data.

The experimental SAR data are processed by the method proposed in this paper, and the results are shown in Figures 2–5. Figure 2 shows the frequency spectrum and time frequency spectrum of SAR echo without interference, respectively. There is no obvious impulse in frequency spectrum. In the time frequency domain, the echo takes
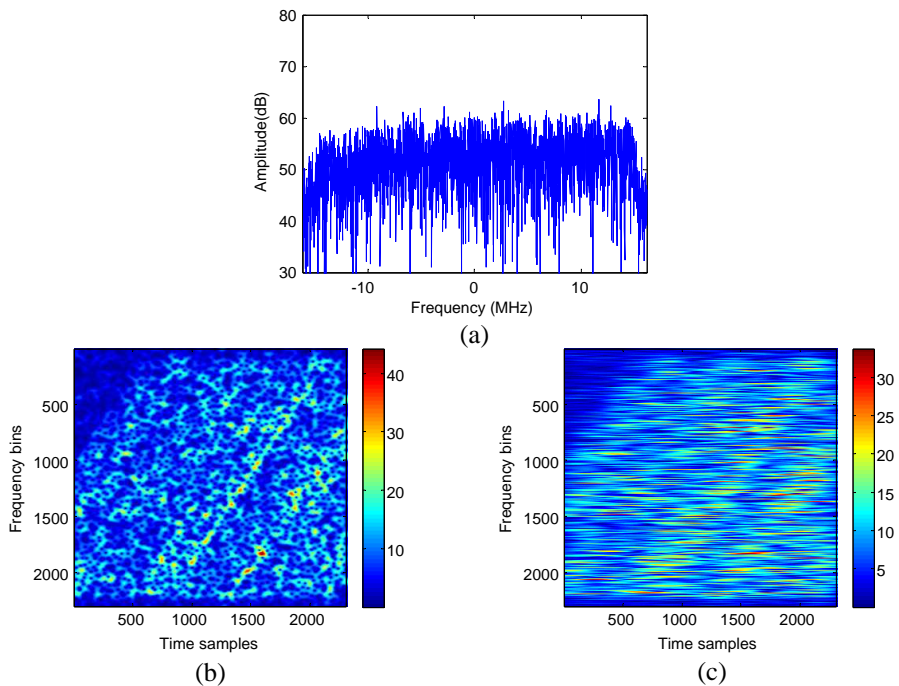


**Figure 2.** Analysis of the clean SAR signal. (a) Frequency spectrum. (b) Time frequency spectrum (window length = 100). (c) Time frequency spectrum (window length = 576).
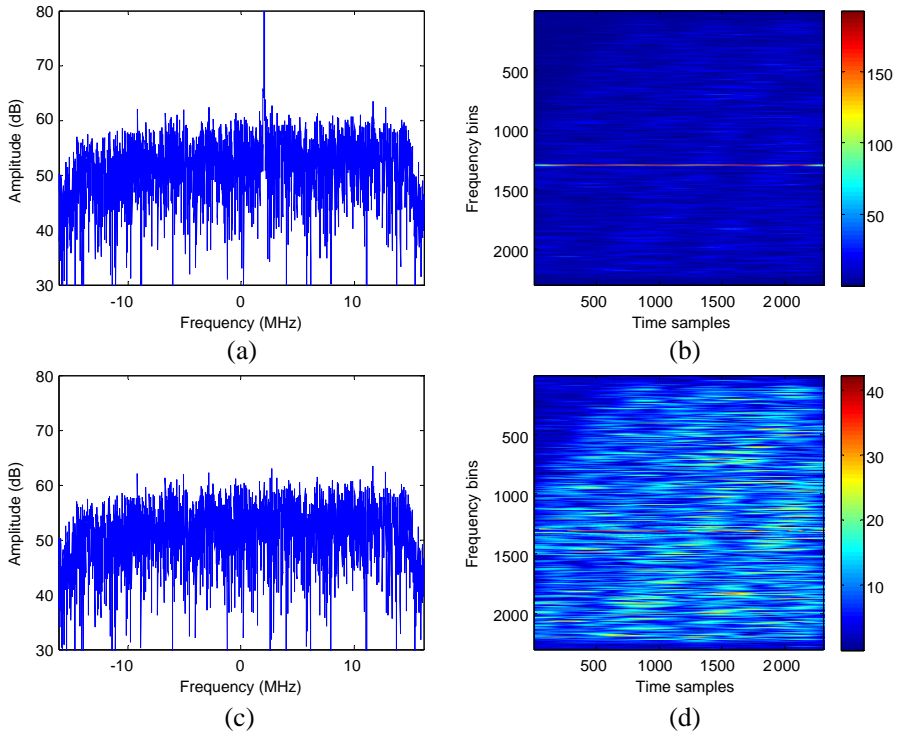
**Figure 3.** Analysis of the SAR signal with NBI (window length = 576 for STFT). (a) Frequency spectrum with NBI. (b) Time frequency spectrum with NBI. (c) Frequency spectrum after interference suppression. (d) Time frequency spectrum after interference suppression.

on noise distribution. The SAR signals with NBI, LFM WBI and DVB-T WBI before and after interference suppression are depicted in Figures 3–5. NBI takes on impulse in the frequency spectrum and narrow bright strip along the time axis in time frequency spectrum. WBI takes on band characteristic in frequency spectrum but the local characteristic in time frequency spectrum. It is obvious that RFI has been suppressed extremely, and SAR signal has been kept correctly in Figure 3(c), Figure 4(c) and Figure 5(c). However, there are still little interference residuals, which can be recognized in Figure 3(d), Figure 4(d) and Figure 5(d).

For the whole SAR data, a comparison among frequency notch filtering, method proposed in [8] and STFT filtering proposed in this paper (the three methods are all based on the notch concept) is
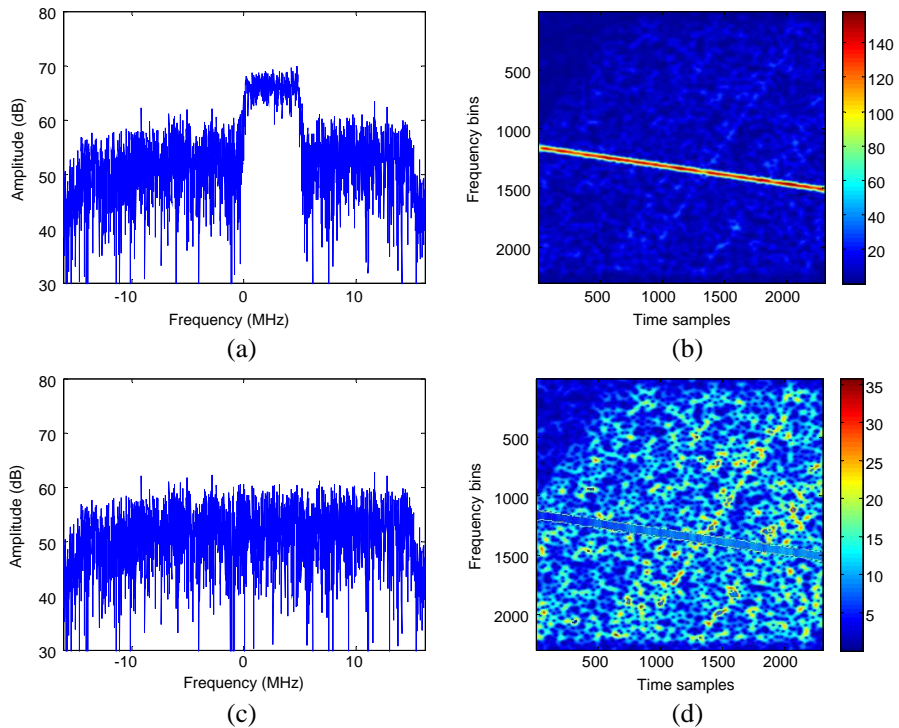
**Figure 4.** Analysis of the SAR signal with NBI (window length = 576 for STFT). (a) Frequency spectrum with NBI. (b) Time frequency spectrum with NBI. (c) Frequency spectrum after interference suppression. (d) Time frequency spectrum after interference suppression.

performed. Figure 6 depicts the clean SAR image, which is in an area of Vancouver, Canada. The details in the image are clear. The SAR images with NBI, LFM WBI and DVB-T WBI after interference suppression are depicted in Figures 7–9. Figure 7 shows good results of the three methods in NBI suppression. The details covered by the NBI are recovered, and the image contrast is enhanced. Figure 8(b) and Figure 9(b) reveal the poor performance of frequency notch filtering in WBI suppression. There are large interference residuals, and the details in the image are still buried by the interference. Figure 8(c) depicts good performance of the method proposed in [8] in LFM WBI suppression, but Figure 9(c) shows the poor performance in DVB-T WBI suppression. Because of the wide spikes in instantaneous frequency spectrum, the wavelet coefficient corresponding to the interference will not be derived exactly. The STFT filtering proposed
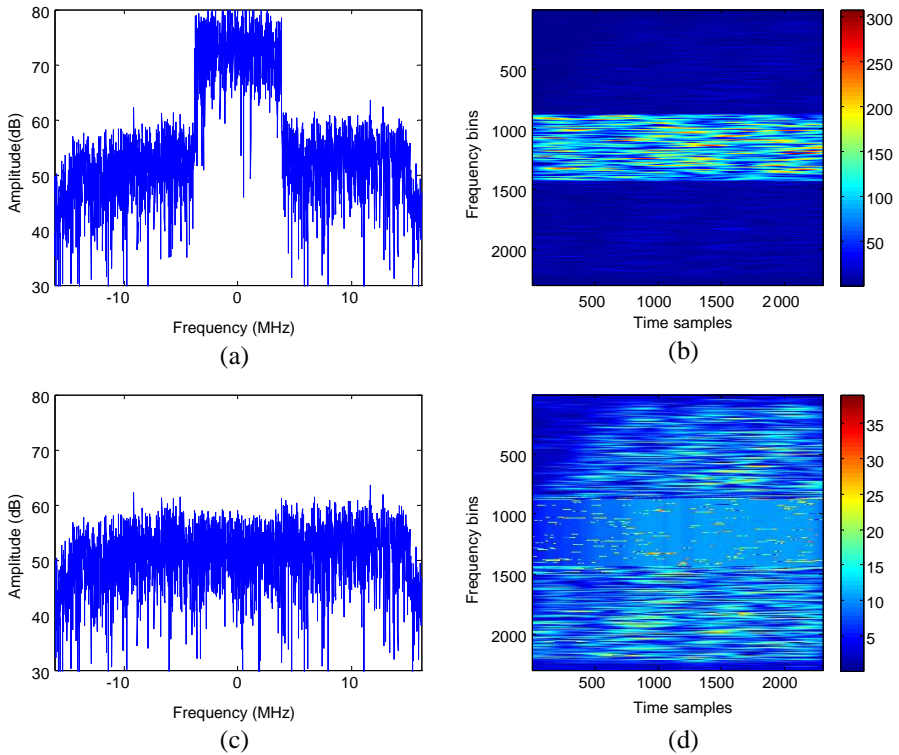
**Figure 5.** Analysis of the SAR signal with DVB-T WBI (window length = 576 for STFT). (a) Frequency spectrum with DVB-T WBI. (b) Time frequency spectrum with DVB-T WBI. (c) Frequency spectrum after interference suppression. (d) Time frequency spectrum after interference suppression.
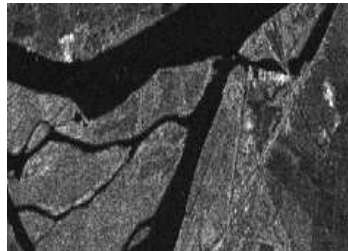


**Figure 6.** The clean SAR image.

in this paper, by contrast, obtains good performance in all NBI, LFM WBI and DVB-T WBI suppression. The WBI will be directly located in time frequency domain and processed by the adaptive gain
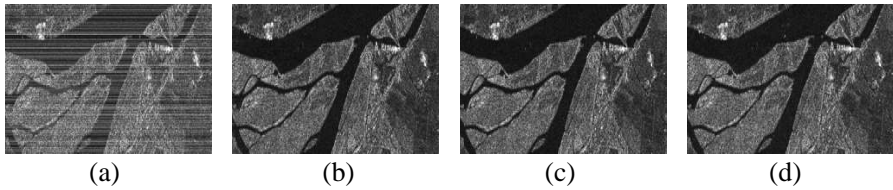
**Figure 7.** The SAR image with NBI after interference suppression.
(a) Before suppression. (b) Frequency notch filtering. (c) Method
proposed in [8]. (d) STFT filtering.
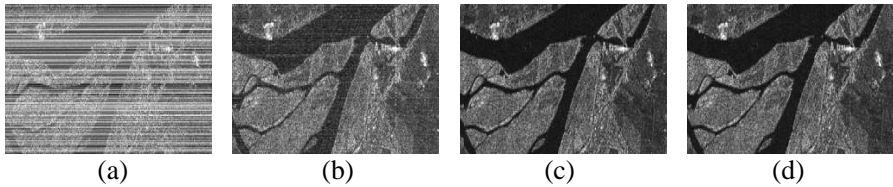


**Figure 8.** The SAR image with LFM WBI after interference
suppression. (a) Before suppression. (b) Frequency notch filtering.
(c) Method proposed in [8]. (d) STFT filtering.
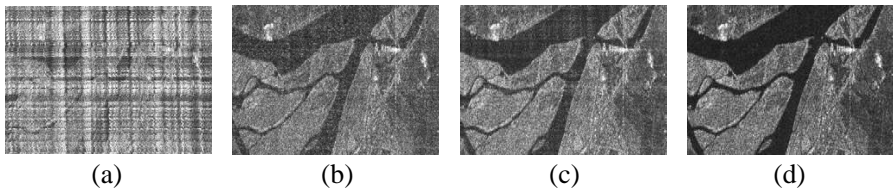


**Figure 9.** The SAR image with DVB-T WBI after interference
suppression. (a) Before suppression. (b) Frequency notch filtering.
(c) Method proposed in [8]. (d) STFT filtering.

coefficient. The results of experiments demonstrate the effectiveness
of the method proposed in this paper. In the next part, we will adopt
two evaluation criterions for the evaluation of interference suppression
effect.

## 4.2. Results Analysis

In order to make a quantitative evaluation for the SAR image after RFI
suppression, this paper will adopt two evaluation criterions: equivalent
number of looks (ENL) and dynamic rang (D) [24]. The ENL is a
criterion to evaluate the intensity of speckle noise in image, and it can
be defined as

$$ENL = \mu^2/\sigma^2 \tag{17}$$

where $\mu$ and $\sigma^2$ denote the statistic mean value and variance of image gradation, respectively. Supposing that the image has $P \times Q$ pixels and that $I_{pq}$ is the gradation value in $(p, q)$ pixel, then

$$\mu = \frac{1}{PQ} \sum_{p=1}^{P} \sum_{q=1}^{Q} I_{pq} \qquad (18)$$

$$\sigma^2 = \frac{1}{PQ} \sum_{p=1}^{P} \sum_{q=1}^{Q} (I_{pq} - \mu)^2 \qquad (19)$$

The ENL reflects the contrast of image gradation. The bigger the ENL is, the smaller the contrast of image gradation is. RFI suppression can decrease the ENL of SAR image and enhance the SAR image contrast.

$D$ can be defined as

$$D = 10 \lg \left( \frac{I_{\max}}{I_{\min}} \right) \qquad (20)$$

where $I_{\max}$ and $I_{\min}$ denote the maximum gradation and minimum gradation of image. $D$ reflects the identifiable ability of strong and weak signals in SAR image (identifiable ability of backscattering coefficient in area). The bigger the $D$ is, the better the image becomes. Table 1 illustrates the quantitative evaluation results of SAR image before and after RFI suppression. It is recognized that all the three methods work well in NBI suppression. However, the frequency notch filtering performs poorly in WBI suppression. The method proposed in [8] performs well in LFM WBI suppression but poorly in DVB-T WBI suppression. By contrast, the method proposed in this paper works well in all NBI, LFM WBI and DVB-T WBI suppression. The results of evaluation also demonstrate the effectiveness of the method proposed in this paper.

## 4.3. Analysis of Computation Load

The computation load among the frequency notch filtering, the method proposed in [8] and the approach proposed in this paper is analyzed.

For the fast Fourier transform (FFT), the computation load $M_{FFT}$ is

$$M_{FFT} = O(N_t \log_2 N_t) \qquad (21)$$

where $N_t$ denotes the length of signal. The computation load of the inverse fast Fourier transform (IFFT) is similar to FFT. Accordingly, the computation loads of STFT and ISTFT are similar, and $M_{STFT}$ is

$$M_{STFT} = O(N_t N_w \log_2 N_w) \qquad (22)$$

**Table 1.** RFI suppression effect evaluation.

| SAR image | ENL | $D$ (dB) |
|---|---|---|
| Without interference | 0.8955 | 54.9655 |
| With NBI | 1.5492 | 46.9840 |
| With NBI after frequency notch filtering | 0.9042 | 52.6428 |
| With NBI after filtering by method in [8] | 0.9071 | 54.9348 |
| With NBI after STFT filtering | 0.9254 | 54.5030 |
| With LFM WBI | 2.5156 | 49.7153 |
| With LFM WBI after frequency notch filtering | 1.3052 | 51.9472 |
| With LFM WBI after filtering by method in [8] | 0.9398 | 53.9795 |
| With LFM WBI after STFT filtering | 0.9606 | 53.7711 |
| With DVB-T WBI | 2.3034 | 49.7327 |
| With DVB-T WBI after frequency notch filtering | 1.5789 | 48.1161 |
| With DVB-T WBI after filtering by method in [8] | 1.4083 | 49.2925 |
| With DVB-T WBI after STFT filtering | 1.1016 | 52.9587 |

where $N_w$ denotes the length of the data window. The computation loads of wavelet transform (WT) and inverse wavelet transform (IWT) are similar, and $M_{WT}$ is

$$M_{WT} = O(HN) \tag{23}$$

where $H$ and $N$ denote the length of window and the length of signal, respectively. For the interference identification, the frequency notch filtering needs $O(N_f)$; the method in this paper needs $O(N_t N_f)$; the method in [8] needs $O(N_t N_{WT})$, where the $N_f$ and $N_{WT}$ denote the number of frequency bins and the wavelet coefficients.

From the above, the computation load of the frequency notch filtering is

$$M_{notch} = O[2 * (N_t \log_2 N_t)] + O(N_f) \tag{24}$$

The computation load of the method in [8] is

$$M_{[8]} = O[2 * (N_t N_w \log N_w)] + O[2 * (H N_t N_w)] + O(N_t N_{WT}) \tag{25}$$

The computation load of the method in this paper is

$$M_{all} = O[2 * (N_t N_w \log_2 N_w)] + O(N_t N_f) \tag{26}$$

During the processing, $N_f$ is equal to $N_w$.

From (24), (25) and (26), it can be seen that the computation load of the method proposed in this paper is higher than the frequency notch filtering, but much lower than the method proposed in [8]. Table 2 illustrates the computation load among the three methods

in the experiment. The SAR data are a 1536-by-2304 matrix. The central processing unit (CPU) and the random access memory (RAM) of computer are Intel (R) Core (TM) i5-2300 and 8GB, respectively. The high performance and efficiency of STFT filtering proposed in this paper are verified in theory and practice.

**Table 2.** Analysis of computation load.

| | Computation load (s) | | |
|---|---|---|---|
| | NBI | LFM WBI | DVB-T WBI |
| Frequency notch filtering | 4 | 4 | 4 |
| STFT filtering | 5729 | 2673 | 5806 |
| Method in [8] | 17818 | 15053 | 19821 |

## 5. CONCLUSION

In this paper, an improved RFI suppression method for SAR based on STFT is proposed. In time frequency spectrum, the interference spot can be located correctly by MMR threshold criterion, and every instantaneous frequency spectrum is processed with an adaptive gain coefficient. The cleaned SAR data can be reconstructed by ISTFT.

The performance of the proposed method is demonstrated by NBI, LFM WBI and DVB-T WBI suppression and excels the frequency notch filtering. Compared with the method proposed in [8], the performance of the proposed method in this paper is similar in both NBI and LFM WBI suppression but better in the DVB-T WBI suppression. Then, two evaluation criterions are used for the quantitative evaluation of interference suppression. In addition, the proposed method in this paper has higher computation efficiency than the method proposed in [8]. From the above, both experimental results and analysis have proven the effectiveness of the proposed method.

## ACKNOWLEDGMENT

## REFERENCES

1. Chan, Y. K. and V. C. Koo, "An introduction to synthetic aperture radar (SAR)," *Progress In Electromagnetics Research B*, Vol. 2, 27–60, 2008.

2. Zhou, W., J. T. Wang, H. W. Chen, and X. Li, "Signal model and moving target detection based on MIMO synthetic aperture radar," *Progress In Electromagnetics Research*, Vol. 131, 311–329, 2012.

3. Mohammadpoor, M., R. S. Abdullah, A. Ismail, and A. Abas, "A circular synthetic aperture radar for on-the-ground object detection," *Progress In Electromagnetics Research*, Vol. 122, 269–292, 2012.

4. Sabry, R., "A novel field scattering formulation for polarimetric synthetic aperture radar: 3D scattering and stokes vectors," *Progress In Electromagnetics Research M*, Vol. 27, 129–150, 2012.

5. Mohammadpoor, M., R. S. Abdullah, A. Ismail, and A. Abas, "Foreign object detection based on circular bistatic synthetic aperture radar," *Progress In Electromagnetics Research M*, Vol. 134, 301–322, 2013.

6. Chan, Y. K. and S. Y. Lim, "Synthetic aperture radar (SAR) signal generation," *Progress In Electromagnetics Research B*, Vol. 1, 269–290, 2008.

7. Zhou, F., R. Wu, M. Xing, and Z. Bao, "Eigensubspace-based filtering with application in narrow-band interference suppression for SAR," *IEEE Geosci. Remote Sens. Lett.*, Vol. 4, No. 1, 75–79, 2007.

8. Zhang, S., M. Xing, R. Guo, L. Zhang, and B. Zheng, "Interference suppression algorithm for SAR based on time-frequency transform," *IEEE Trans. Geosci. Remote Sens.*, Vol. 49, No. 10, 3765–3779, 2011.

9. Chang, W., M. Cherniakov, X. Li, and J. Li, "Performance analysis of the notch filter for RF interference suppression in ultra-wideband SAR," *Proc. ICSP*, 2446–2451, 2008.

10. Dong, Z., D. Liang, and X. Huang, "A RFI suppression algorithm based on channel equalization for the VHF/UHF UWB SAR," *Journal of Electronics & Information Technology*, Vol. 30, No. 3, 550–553, 2008.

11. Lord, R. T. and M. R. Inggs, "Approaches to RF interference suppression for VHF/UHF synthetic aperture radar," *Proc. COMSIG*, 95–100, 1998.

12. Yu, C., Y. Zhang, Z. Dong, and D. Liang, "SVD-based methods for radio frequency interference applied to SAR," *Defence Science Journal*, Vol. 62, No. 2, 132–136, 2012.

13. Huang, N. E., Z. Shen, S. R. Long, M. C. Wu, H. H. Shih, and Q. Zheng, "The empirical mode decomposition and the Hilbert

spectrum for non-linear and non-stationary time series analysis," *Proc. R. Soc. Lond. A, Math. Phys. Sci.*, Vol. 454, 903–995, 1998.

14. Feng, Z., M. Xing, X. Bai, G. Sun, and Z. Bao, "Narrow-band interference suppression for SAR based on complex empirical mode decomposition," *IEEE Geosci. Remote Sens. Lett.*, Vol. 6, No. 3, 423–427, 2009.

15. Jin, F., H. Zheng, Y. Deng, and D. Gao, "Application of subband spectral cancellation for SAR narrow-band interference suppression," *IEEE Geosci. Remote Sens. Lett.*, Vol. 9, No. 2, 190–193, 2012.

16. Reigber, A. and L. Ferro-Famil, "Interference suppression in synthesized SAR images," *IEEE Geosci. Remote Sens. Lett.*, Vol. 2, No. 1, 45–49, 2005.

17. Perez-Solano, J. J., S. Felici-Castell, and M. A. Rodriguez-Hernandez, "Narrowband interference suppression in frequency-hopping spread spectrum using undecimated wavelet packet transform," *IEEE Trans. Veh. Technol.*, Vol. 57, No. 3, 1620–1629, 2008.

18. Huang, X. and D. Liang, "Gradual RELAX algorithm for RFI suppression in UWB-SAR," *Electron. Lett.*, Vol. 35, No. 22, 1916–1917, 1999.

19. Goodberlet, M. A. and I. Popstefanija, "RFI mitigation using two-scale estimators for statistical variance," *IEEE Geosci. Remote Sens. Lett.*, Vol. 10, No. 4, 721–725, 2013.

20. Miller, T., L. Potter, and J. McCorkle, "RFI suppression for ultra wideband radar," *IEEE Trans. Aerosp. Electron. Syst.*, Vol. 33, No. 4, 1142–1156, 1997.

21. Digital Video Broadcasting (DVB), Framing Structure, Channel Coding and Modulation for Digital Terrestrial Television (DVB-T), ETSI Standard 300 744, 1997.

22. Ouyang, X. and M. G. Amin, "Short-time Fourier transform receiver for non-stationary interference excision in direct sequence spread spectrum communications," *IEEE Trans. Signal Process.*, Vol. 49, No. 4, 851–863, 2001.

23. "Mitigation technique to facilitate the use of the 1215–1300 MHz band by the Earth exploration-satellite service (active) and the space research service (active)," Rec. ITU-R RS. 1749, 2006.

24. Yu, C., "Study on active interference suppression for synthetic aperture radar," Ph.D Dissertation, Department of Electronics Science and Engineering, National University of Defense Technology, 2012.